15TH IEA HEAT PUMP CONFERENCE
MAY 26–29, 2026 | HOFBURG
VIENNA 2026
DECARBONISATION THROUGH INNOVATION

A novel Model Predictive Control framework for replacing traditional on-board Heat Pump controls

Alice Mugnini[a*], Alessia Arteconi[b,c]

[a]Department of Theoretical and Applied Sciences, Università E-Campus, Novedrate 22060, Italy
[b]Department of Mechanical Engineering, KU Leuven 3001, Belgium
[c]EnergyVille, Genk 3600, Belgium

Abstract

Heat pumps are a key technology for decarbonization and enabling demand-side flexibility. Fully realizing this potential requires advanced, model-based control strategies capable of responding to specific signals and anticipating system behaviour through predictive models of both thermal demand and heat pump performance. While significant progress has been made in modelling techniques for control systems, the integration of dynamic heat pump models within this framework remains an area requiring further development. Heat pumps are often modeled using performance curves in control systems, but such representations neglect onboard controls, which significantly affect performance and are typically inaccessible to end users. Addressing this issue requires detailed models that simulate the thermodynamic vapor cycle of each heat pump component. A common approach in the literature employs state-space representations of the thermodynamic cycle, using heat exchanger models such as Moving Boundary Models. However, these models are computationally intensive and often too complex for real-time dynamic control applications.
This study provides a first demonstration of how the state-space formulation of the heat pump can be adapted for control applications. A black-box modeling approach is employed to represent the thermodynamic properties of the refrigerant, while linearization techniques are used to assess their impact on computational efficiency. Based on this approach, a new Model Predictive Control framework is proposed, using a linearized vapor-cycle model with Moving-Boundary heat exchanger representations. The framework is designed to act as a lower-level controller that replaces the on-board controllers typically used in heat pumps. The new control strategy has been implemented for a case study and tested in a simulation environment to evaluate its ability to track setpoints. The results demonstrate the effectiveness of the approach and provide a preliminary assessment of its potential, limitations, and future challenges.

Selection and/or peer-review under the responsibility of the organizers of the 15th IEA Heat Pump Conference 2026.

Keywords: Heat Pump; Model Predictive Control; On board control; Moving Boundary Model; Linearization

1. Introduction

Heat pumps (HPs) represent a pivotal technology for achieving Europe's climate neutrality objectives by 2050 [1]. Electrically driven HPs provide a highly efficient alternative to conventional fossil-fuel boilers, thereby supporting the electrification of thermal demand, which in turn facilitates the integration of renewable energy sources and enhances energy system flexibility through the controllable management of thermal loads [2]. In particular, energy flexibility refers to the ability of an energy system to adjust its demand and generation in response to local climate conditions, user requirements, and power grid constraints [3]. This capability is especially important in systems with a high share of non-dispatchable renewable energy sources, as it allows the system to operate safely and reliably under variable conditions.

* Corresponding author. Tel.:
E-mail address: alice.mugnini@uniecampus.it

To exploit the energy flexibility potential of an HP system, two main aspects are required. First, a sufficient level of thermal inertia must be available to decouple thermal energy demand from electrical generation. Second, an advanced control strategy capable of real-time system management in a flexible manner is essential.

Many studies have demonstrated that HP-based systems [4, 5], particularly when integrated with building heating and cooling installations, offer multiple sources of thermal inertia that can be harnessed to provide energy flexibility, for instance, through the building's thermal mass [6] or dedicated storage systems [7]. From a control perspective, high-level supervisory controllers are required to respond to external signals (e.g., price or demand-response signals) and to optimally coordinate HP operation to meet specific objectives under given system constraints [8]. Such control relies on predictive capabilities supported by dynamic models of thermal demand and HP performance. Among the various approaches, Model Predictive Control (MPC) has emerged as one of the most widely adopted methodologies [9]. MPC employs a dynamic representation of the system to predict future behaviour and compute optimal control actions that minimize a defined objective function while accounting for disturbances and operational constraints [10].

Numerous studies have further highlighted the effectiveness of a high-level MPC in enhancing thermal demand flexibility through HP operation. For example, Tomás et al. [11] demonstrated that implementing MPC in a low-energy non-residential building can reduce energy costs by up to 40% and increase the grid support coefficient by 13%. Similarly, Zhao et al. [12] investigated the use of adaptive MPC in a HP-assisted solar water heating system, reporting cost savings of 20% and energy savings of 12% compared to conventional Proportional–Integral–Derivative (PID) control. In another study, Strauch et al. [13] analyzed MPC implementation in a residential building equipped with distributed energy resources, including photovoltaics, battery storage, an electric vehicle, and HP, and showed that under real-time pricing, MPC can reduce peak demand and overall energy costs by up to 92% and 28%, respectively, relative to the baseline.

Although the potential of a high-level MPC to enable thermal demand flexibility has been widely demonstrated, several barriers still limit its large-scale deployment [14]. A primary challenge is that most MPC implementations rely on HP models derived from performance curves, which often neglect the short-term dynamics introduced by low-level on-board control. Experimental evidence shows that these on-board dynamics can significantly affect system flexibility, with discrepancies in predicted electrical consumption exceeding 10% across different control strategies [15,16].

Traditionally, on-board controls use conventional Proportional–Integral–Derivative (PID) controllers or pre-programmed logics to manage compressors, valves, and pumps safely. However, these embedded controllers are often inaccessible, difficult to integrate with high-level supervisory control, and inherently rigid, imposing strong operational constraints that limit the flexibility of a high-level MPC. Achieving more flexible control requires a low-level control strategy that can interact directly with the high-level MPC, which in turn necessitates the use of advanced control techniques, such as MPC applied also at the on-board level. Consequently, predictive models capable of simulating the thermodynamic behavior of each HP component are essential. While common approaches, such as state-space models with detailed Moving Boundary Models (MBMs) [17–19], are effective in simulation, they are often too computationally intensive for real-time implementation, highlighting the need for simplified yet accurate predictive models suitable for low-level MPC design.

Given the current lack of studies addressing on-board control effects in high-level MPC and the inherent complexities of dynamic thermodynamic cycle modeling, a novel low-level MPC framework is proposed to replace traditional on-board logics for managing the vapor-compression cycle. The framework is designed to enable more flexible system operation and facilitate future integration with high-level supervisory control. The low-level MPC uses control-oriented modelling techniques widely recognized in the literature, particularly MBMs, with simplifications such as linearization and black-box property estimation to reduce computational load. Their application within a low-level MPC constitutes a novel framework, significantly lowering computational complexity compared to traditional simulation use.

In this paper, the proposed control strategy is presented methodologically and tested in a simulation environment on a case study to evaluate its ability to track setpoints. The aim of this work is to provide a first demonstrative study that validates the applicability of the proposed low-level control approach and describes its practical implementation. Future research will focus on integrating this framework within a high-level controller for coordinated system management.

2. Methodology

In this section, the methodology for implementing the proposed low-level MPC control framework is presented. The methodology consists of two main parts, corresponding to the different phases of the control strategy. In the first phase, the thermodynamic cycle is simulated using a high-fidelity model, and black-box modeling techniques are employed to derive correlations for the thermodynamic properties of the refrigerant. Subsection 2.1 provides a detailed description of this phase. Subsequently, the high-fidelity model is linearized around the equilibrium point obtained from the simulation. From this linearization, a Linear Time-Invariant (LTI) model is constructed, which serves as the predictive model in a traditional MPC scheme. The MPC aims to control the superheat at the evaporator outlet and the secondary fluid temperature at the condenser outlet by manipulating the compressor speed and the expansion valve opening. This approach is described in detail in subsection 2.2. These two phases are carried out within the Prediction Horizon (PH) of the MPC and applied to the system at each control timestep following the receding horizon principle, as detailed in subsection 2.2. Figure 1 provides a general overview of the controller operation and its main functional blocks.

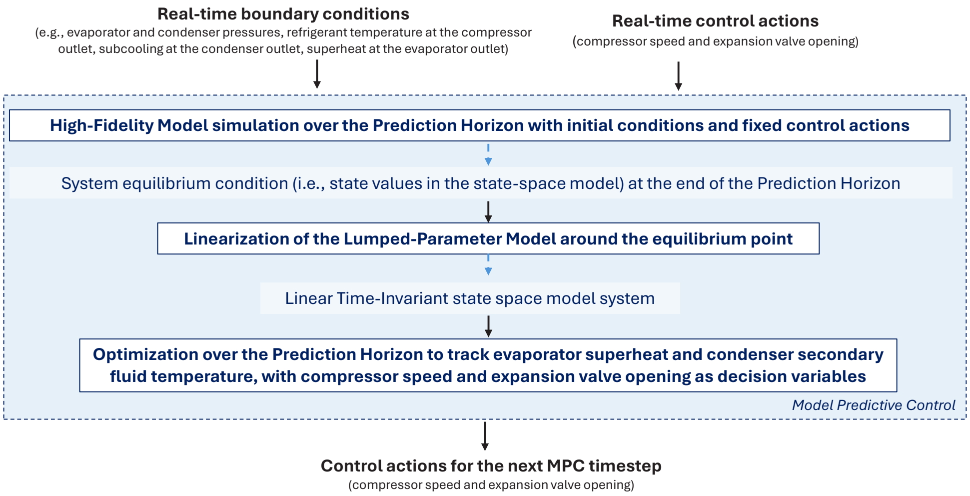

Figure 1. Overview of the MPC framework.

2.1 High-Fidelity Modeling and Black-Box Correlation Development

In this section, the dynamic high-fidelity model used in the initial phase of MPC (Figure 1) is described. The modelling adopts a Lumped Parameter Model (LPM) with a MBM for the heat exchangers, chosen as a trade-off between accuracy and computational efficiency, while semi-empirical models are employed for the expansion valve and the compressor, as reported in the literature [20, 21, 22]. The complex geometries of the heat exchangers were simplified into equivalent pipe-in-pipe models, preserving accuracy while reducing computational costs. Although more efficient than other high-fidelity approaches, such as Finite Volume Methods [23], LPMs remain computationally demanding for real-time MPC, mainly due to the retrieval of refrigerant properties through *CoolProp* [24] in Python, where the entire model was developed to ensure open-source accessibility. Previous studies indicate that the computation time required to determine control actions should not exceed half of the MPC timestep duration [25]. Therefore, to ensure compatibility with the controller, a black-box modeling approach was adopted to derive semi-empirical correlations for refrigerant properties, thereby reducing simulation times to levels consistent with the PH. This aspect will be further clarified in the discussion of the results. Subsection 2.2.1 presents the models developed for each component of the high-fidelity model, while Subsection 2.2.2 outlines the techniques implemented to further accelerate the simulation of the LPM.

2.1.1 Component Models of the High-Fidelity Simulation

The HP system consists of four main components: the heat exchangers (i.e., evaporator and condenser), the expansion valve, and the compressor. The modelling techniques adopted for each component are derived from scientific literature; therefore, only the fundamental aspects are presented here. For further details, the reader is referred to the original sources [17–22].

The heat exchangers are modelled using the lumped-parameter MBM, a high-fidelity approach that offers a significantly lower computational cost compared to distributed-parameter methods such as finite volume models, being up to three times faster at comparable accuracy [23]. In the MBM, each heat exchanger is represented in state-space form, dividing it into zones corresponding to specific refrigerant phases. The evaporator is divided into two zones, a two-phase region and a superheated vapor region, whereas the condenser comprises three zones: superheated vapor, two-phase, and subcooled liquid. The interface between zones (identified by the length L of the section occupied by each) varies over time according to the system dynamics. Treating the two-phase region as a single zone is made possible by adopting a key simplifying assumption: the mean void fraction ($\bar{\gamma}$) is considered approximately constant. This assumption is supported by Wedekind et al. [26], who demonstrated that the mean void fraction remains largely invariant under most operating conditions. Consequently, although the position of the dry-out point or the interface between zones may shift with changing inlet conditions, the liquid–vapor distribution within the two-phase region remains essentially unchanged.

MBM applies the conservation equations of mass, refrigerant energy, and wall energy to each zone, while neglecting momentum balance due to the minimal influence of pressure drops and viscous effects. Complex heat exchanger geometries (e.g., shell-and-tube, plate, or shell-and-plate configurations) are represented as concentric tube-in-tube systems, assuming predominantly one-dimensional flow, negligible axial conduction, and accounting for the thermal capacitance of the wall material while neglecting its thermal resistance. Figure 2 illustrates the schematic representation of the heat exchangers according to the MBM model (Figure 2a the evaporator and Figure 2b the condenser). For brevity, the complete equations are not explicitly reported here; however, the figure provides a clear understanding of the overall configuration of the system (the complete set of equations can be found in [17–22]).

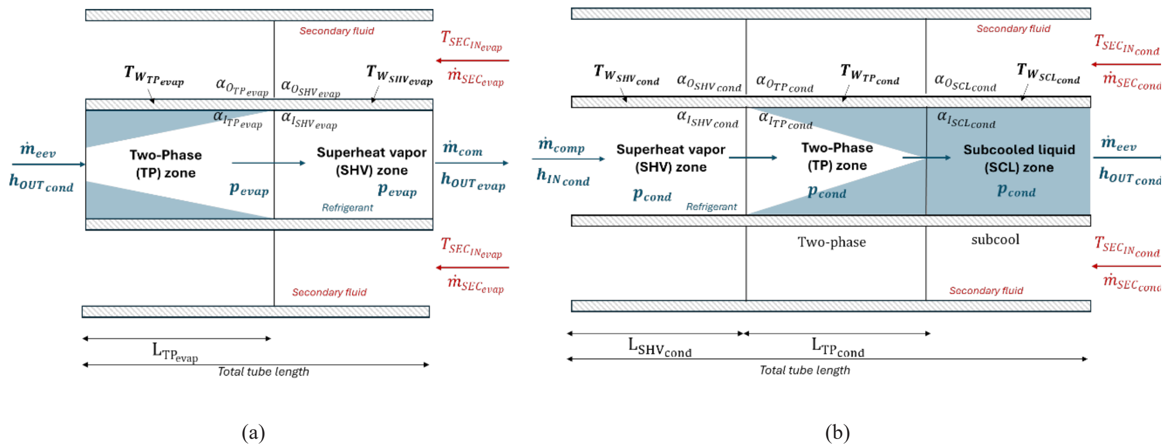

Figure 2. Schematic representation of the heat exchangers (tube-in-tube configuration) according to the MBM model: (a) evaporator and (b) condenser.

In the case of the evaporator, the dynamic behavior is described in state-space form by five state variables (X_{evap}), grouped in the vector presented in Eq. (1).

$$\mathrm{X}_{evap} = \begin{bmatrix} L_{TP_{evap}} & p_{evap} & h_{OUT\,evap} & T_{W_{TP_{evap}}} & T_{W_{SHV_{evap}}} \end{bmatrix}^T \tag{1}$$

Where $L_{\mathrm{TP,\,evap}}$ is the length of the Two-Phase (TP) region, p_{evap} is the evaporator pressure, $h_{\mathrm{OUT,\,evap}}$ is the outlet specific enthalpy of the refrigerant, $T_{W,\mathrm{TP,\,evap}}$ is the wall temperature in the TP region, and $T_{W,\mathrm{SHV,\,evap}}$ is the wall temperature in the Superheated Vapor (SHV) region.

For the condenser, the dynamic behavior is described in state-space form by seven state variables (X_{cond}), grouped in the vector presented in Eq. (2):

$$\mathrm{X}_{cond} = \begin{bmatrix} L_{SCL_{cond}} & L_{TP_{cond}} & p_{cond} & h_{OUT\,cond} & T_{W_{SCL_{cond}}} & T_{W_{TP_{cond}}} & T_{W_{SHV_{cond}}} \end{bmatrix}^T \tag{2}$$

Here, $L_{\mathrm{SCL,\,cond}}$ is the length of the Subcooled Liquid (SCL) region, $L_{\mathrm{TP,\,cond}}$ is the length of the TP region, p_{cond} is the condenser pressure, $h_{\mathrm{OUT,\,cond}}$ is the outlet specific enthalpy of the refrigerant, $T_{W,\mathrm{SCL,\,cond}}$ is the wall temperature in the SCL, $T_{W,\mathrm{TP,\,cond}}$ is the wall temperature in the TP region, and $T_{W,\mathrm{SHV,\,cond}}$ is the wall temperature in the SHV region.

The inputs required for the heat exchanger models are the mass flow rates of the secondary fluids entering the exchangers ($\dot{m}_{\mathrm{SEC,\,evap}}$ for the evaporator and $\dot{m}_{\mathrm{SEC,\,cond}}$ for the condenser) and the inlet temperatures of the secondary fluids ($T_{\mathrm{SEC,\,IN,\,evap}}$ for the evaporator and $T_{\mathrm{SEC,\,IN,\,cond}}$ for the condenser).

The heat transfers between the refrigerant and the heat exchanger tube wall, and between the tube wall and the secondary fluid, are evaluated using heat transfer coefficients (α), as indicated in Figure 2. In the condenser, in the SCL region the internal tube coefficient is $\alpha_{I,\mathrm{SCL,\,cond}}$ and the external coefficient toward the secondary fluid is $\alpha_{O,\mathrm{SCL,\,cond}}$; in the TP region, the coefficients are $\alpha_{I,\mathrm{TP,\,cond}}$ and $\alpha_{O,\mathrm{TP,\,cond}}$, while in the SHV region they are $\alpha_{I,\mathrm{SHV,\,cond}}$ and $\alpha_{O,\mathrm{SHV,\,cond}}$.

In the evaporator, in the TP region the internal coefficient is $\alpha_{I,\mathrm{TP,\,evap}}$ and the external coefficient is $\alpha_{O,\mathrm{TP,\,evap}}$, while in the SHV region the corresponding coefficients are $\alpha_{I,\mathrm{SHV,\,evap}}$ and $\alpha_{O,\mathrm{SHV,\,evap}}$. All values of the coefficients α are obtained from experimental correlations available in the literature; further details will be provided in Section 3, where the case study is presented.

Regarding the expansion valve (i.e., Electronic Expansion Valve EEV), it is modeled using the semi-empirical approach proposed by Li [27], which describes the refrigerant mass flow as:

$$\dot{m}_{\mathrm{eev}} = C_D A Y \sqrt{2\rho_i P_i X} \tag{3}$$

where $\dot{m}_{\mathrm{eev}}$ is the refrigerant mass flow, C_D is the discharge coefficient which is a function of the valve opening fraction z, A is the valve opening area (m^2), and ρ_i and P_i are the inlet refrigerant density (kg m^{-3}) and pressure. P_o is the outlet pressure (Pa), and X and Y are defined as:

$$X = \frac{P_i - P_o}{P_i}, \qquad Y = 1 - \frac{X}{3F_Y X_T}, \qquad F_Y = \frac{k}{1.4} \tag{4}$$

where k is the specific heat ratio of the refrigerant and X_T is a valve-specific parameter determined experimentally. The coefficients C_D and X_T are based on experimental data, making the model semi-empirical.

Regarding the compressor, the mass flow rate ($\dot{m}_{\mathrm{com}}$) is calculated as:

$$\dot{m}_{\mathrm{com}} = \omega V_{\mathrm{com}} \rho_{\mathrm{in}} C_c \left(\frac{P_{c,o}}{P_{c,i}}\right)^{1/n} \tag{5}$$

where ω is the compressor speed (rps, i.e. revolutions per second), V_{com} is the total displacement volume (m^3 rev^{-1}), ρ_{in} is the refrigerant density at the inlet (kg m^{-3}), and C_c is the ratio of clearance volume to piston displacement. $P_{c,o}$ and $P_{c,i}$ are the outlet and inlet pressures (Pa), and n is the polytropic index, defined as:

$$n = \frac{\ln\,(P_{c,o}/P_{c,i})}{\ln\,(\rho_{\mathrm{out}}/\rho_{\mathrm{in}})} \tag{6}$$

Assuming an isentropic efficiency (or a value provided by the manufacturer), the model also outputs the refrigerant enthalpy at the condenser inlet.

By integrating the component models described previously, a complete system model can be formulated. The input vector of the overall system, U, is defined as:

$$U = \begin{bmatrix} \dot{m}_{SEC_{evap}} & T_{SEC_{IN_{evap}}} & \dot{m}_{SEC_{cond}} & T_{SEC_{IN_{cond}}} & z & \omega \end{bmatrix}^T \tag{7}$$

The global state vector, x, is obtained by combining the states from Equations (1) and (2), resulting in a total of 12 states. The system dynamics matrix D and the function vector f are obtained by assembling the corresponding matrices and functions of the evaporator, condenser, compressor, and EEV models. Thus, the overall system dynamics can be expressed in compact form as:

$$\dot{X} = D^{-1} f(X, U) \tag{8}$$

These equations form a set of nonlinear, dynamic, coupled partial differential equations that yield a unique solution for given initial and boundary conditions and can be solved numerically using methods.

2.1.2 Black-Box Model for High-Fidelity Simulation Acceleration

When developing a control-oriented model, an important aspect, besides prediction accuracy, is the computational time, which must be compatible with the time step of the control system [25]. Some studies [28] have shown that the calculation of the thermophysical properties of refrigerants has the most significant impact on computational speed (ref. Maged). In this study, since the control is implemented in Python to ensure accessibility, *CoolProp* [24] is used to obtain the thermodynamic properties of refrigerants. A challenge that arose, which will also be discussed in the Results section (Section 4), concerns the computational time associated with calling *CoolProp*. To significantly reduce this computational cost, black-box models based on polynomial regression were introduced to represent the thermo-fluid properties of refrigerants. These correlations were trained using data from *CoolProp*. In total, 38 polynomial equations were implemented, adapting the polynomial form to the data to be represented. These equations cover all the thermodynamic properties of the refrigerant across all states and phases (subcooled liquid, saturated liquid, two-phase, saturated vapor, and superheated vapor). As an example, Eq. (9) reports a representative correlation for the density of subcooled liquid (ρ_{SCL}):

$$\rho_{SCL}(P,h) = \sum_{i=0}^{2} a_i P_n^i + (\sum_{i=0}^{2} b_i P_n^i) \cdot (\sum_{j=0}^{2} c_j h_n^j) + \sum_{j=0}^{2} d_j h_n^j \tag{9}$$

where a_i, b_i, c_j, and d_j are polynomial coefficients obtained by regression on *CoolProp* data, and P_n and h_n are the pressure and enthalpy normalized by their respective critical values.

2.2 Linearization and MPC Framework Implementation

An MPC framework essentially consists of two main components: the control-oriented model and the optimizer. Consequently, the model must be solvable within the PH, and the optimizer must be capable of finding a feasible control solution in real time. To achieve a detailed representation of the thermodynamic cycle, a high-fidelity model is required (subsection 2.1). However, despite its accuracy, the MBM is not directly suitable for control applications, as its numerical solution requires extremely short timesteps (e.g., 10^{-6} s) and high computational effort. Therefore, to overcome this limitation, a new control framework has been introduced. Using MBM as a reference, a linearization-based approach is employed to derive a control-oriented model. At each control step (Δk_{MPC}), the MBM is linearized around the predicted operating point within the MPC prediction horizon, resulting in a Linear Time-Invariant (LTI) state-space representation. The nonlinear system is linearized around the equilibrium point (X_{eq}, U_{eq}) by computing the Jacobian matrices of the system dynamics and output functions. Specifically, let *f(x,u)* represent the differential equations describing the system, and *g(x,u)* denote the output functions. The resulting linear model can be expressed as:

$$\dot{X} = AX + BU, \qquad Y = CX + DU \tag{10}$$

where the matrices are defined as:

$$A = \frac{\partial f}{\partial x}\Big|_{(X_{eq},U_{eq})}, \qquad B = \frac{\partial f}{\partial u}\Big|_{(X_{eq},U_{eq})}, \qquad C = \frac{\partial g}{\partial x}\Big|_{(X_{eq},U_{eq})}, \qquad D = \frac{\partial g}{\partial u}\Big|_{(X_{eq},U_{eq})} \tag{11}$$

The linearization is performed numerically using the Python linearize function (i.e., *hp_sys.linearize*), which automatically computes the partial derivatives at the equilibrium point and generates the corresponding state-space model.

Starting from the linearized system, the optimizer efficiently solves the MPC problem. Its main objective is to determine the optimal control actions, specifically the EEV valve opening (z) and the compressor speed (ω), to minimize the deviation of the system outputs from their setpoints, which correspond to the secondary fluid outlet temperature at the condenser and the superheating at the evaporator outlet. The MPC formulation relies on a linearized version of the system, which is first discretized over the sampling time Δk_{MPC} according to:

$$\mathrm{A_d} = \mathrm{e}^{\mathrm{A}\Delta \mathrm{k_{MPC}}}, \qquad \mathrm{B_d} = \mathrm{A}^{-1}(\mathrm{A_d} - \mathrm{I})\mathrm{B} \tag{12}$$

For control purposes, only the subsystem of interest, comprising the manipulated inputs z and ω, is considered, while all other inputs are treated as fixed constants. The MPC operates over a defined PH, with a cost function that penalizes deviations of the outputs from their references through weight matrix Q and the control effort through weight matrix R. Manipulated input constraints are imposed as absolute limits U_{min} and U_{max}, expressed as deviations from the equilibrium inputs U_{eq}. Similarly, the system state is represented in terms of deviations from equilibrium as:

$$X_{dev} = X_0 - X_{eq} \tag{13}$$

Since the system contains nonlinear components, such as the EEV and the compressor, linear sensitivities of the mass flows with respect to the manipulated inputs are computed numerically, i.e., $\partial m_{eev}/\,\partial z$ and $\partial m_{comp}/\,\partial \omega$. These sensitivities are then incorporated into the MPC problem as linear constraints on mass flow deviations, effectively ensuring mass conservation within the linearized framework.
The resulting optimization problem is formulated as a Quadratic Program (QP) and solved using the OSQP solver in Python via *cvxpy*. The objective function minimizes a combination of output deviations, control effort, and optional slack variables s_k used to relax constraints:

$$minimize\left[\sum_{k=0}^{PH}(Y_k - Y_{ref})^{\top}Q(Y_k - Y_{ref}) + U_k^{\top}RU_k + s_k^2 \cdot slack_{weight}\right] \tag{14}$$

This optimization is subject to the discrete-time linearized dynamics

$$miX_{k+1} = A_d X_k + B_{ctrl}U_k + B_{fixed}U_{fixed} \tag{15}$$

as well as input constraints $U_{min} \leq U_k \leq U_{max}$ and mass flow deviation limits $|\,(\partial m_{eev}/\,\partial z)u_0 - (\partial m_{comp}/\,\partial \omega)u_1\,| \leq s_k$, with slack variables constrained to be nonnegative.
Once the QP is solved, the optimal input deviations U_k are converted back to absolute values by adding the equilibrium inputs U_{eq}, and the predicted trajectories of outputs and states are reconstructed in absolute terms as

$$Y_{abs} = Y_{dev} + Y_{eq}, \qquad X_{abs} = X_{dev} + X_{eq} \tag{16}$$

The MPC control is applied according to the receding horizon principle, where only the first action of the computed sequence is implemented at each step. Figure 3 shows an overall schematic representation of the proposed moving linearization process within the MPC framework.

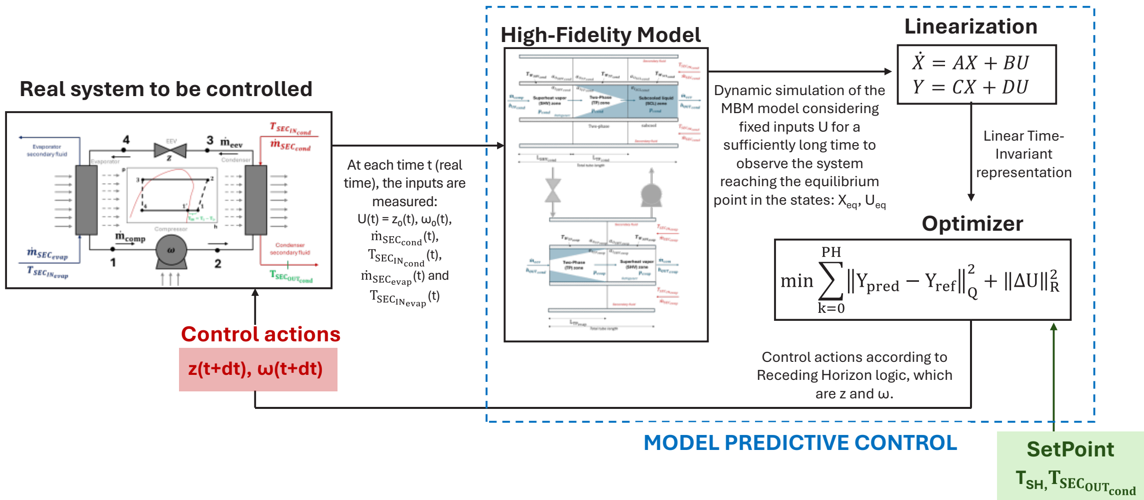

Figure 3. Schematic representation of the moving linearization process within the MPC framework.

3. Case study

The control was tested on a hypothetical high-temperature water–ammonia heat pump, whose characteristics were derived from [29]. The case study concerns an industrial high-temperature heat pump capable of maintaining stable outlet temperatures between 160°C and 200°C, with a maximum temperature lift of 100°C and a thermal power at the condenser of approximately 100 kW_{th}. Due to the unavailability of thermophysical properties for the ammonia–water mixture, simulations were performed using pure water as the refrigerant, which also significantly reduced the simulation time.

The heat exchangers assumed for the simulations were selected based on datasheets of commercially available components (e.g. [30] [31]). The condenser was represented as a shell-and-plate heat exchanger, made of AISI 316L with a plate thickness of approximately 0.8 mm, a diameter of 440 mm, and consisting of 134 plates. The evaporator was represented as a plate heat exchanger, also made of AISI 316L, with plate dimensions of 529 × 271 mm, a thickness of 0.4 mm, and 140 plates in total. As anticipated, to implement the high-fidelity model (Section 2.1), a simplified modelling of the heat exchangers with a concentric tube configuration is required. For this purpose, equivalent concentric tube heat exchangers were estimated for both the condenser and the evaporator, based on the heat duty conditions of the cycle and the geometric data of the real components. Equivalence was defined by ensuring that the heat duty and thermal capacitance of the equivalent exchanger match those of the real one, assuming one-dimensional flow, negligible pressure drops, negligible axial conduction, and negligible material resistance [23]. This results in single-channel lengths of approximately 46.3 m for the evaporator and 51.8 m for the condenser, ensuring consistency between the simplified pipe in pipe model and the actual heat exchangers. To model heat transfer between the fluids and the heat exchanger walls, correlations accounting for the variation of the heat transfer coefficient with operating conditions were used. The secondary fluid used is T66, a commercial heat transfer fluid (e.g., *Therminol 66*) employed in the secondary circuit for heat transfer. In the condenser, correlations for calculating the heat transfer were extrapolated from [32] for the single-phase regions of the refrigerant (SHV and SCL zones) and for the secondary fluid, while Shah's correlation [33] was used for the condensation phase. For the evaporator, correlations for the refrigerant in single-phase (SHV) and for the secondary fluid were extrapolated from [32], whereas for the refrigerant in the evaporation phase, the correlation from [34] was adopted.

Regarding the EEV, the model used is semi-empirical and requires specific parameters, such as the discharge coefficient (C_D) and the pressure differential ratio (X_T), which are normally provided by the manufacturer (Eq. (3)-(4)). Since these values are not available for the real prototype, they were estimated using a semi-empirical curve fitting approach based on experimental data from an R22-based EEV reported by W. Li [27]. The curve data were digitally extracted and scaled to the desired mass flow rate, providing an approximate estimate sufficient to simulate the EEV dynamics, which are much faster than those of the heat exchangers. Regarding the compressor, a clearance volume (C_c in Eq. (5)) of 0.0015 and a compression volume of (V_{comp} in Eq. (5)) of 0.0006882 $m^3\ rev^{-1}$ were assumed. Furthermore, the compressor is considered to have an isentropic efficiency of 0.75.

4. Results and discussion

This section presents the results of applying the proposed low-level MPC framework to the case study described in Section 3. The discussion is divided into two subsections: 4.1 presenting the controller performance, and 4.2 outlining the limitations of the study and potential developments.

4.1 Application Results of the Low-Level MPC Framework

This section presents the results of applying the proposed low-level MPC framework to the case study described in Section 3. In this preliminary study, the controller regulates the secondary fluid outlet temperature from the condenser ($T_{SEC_{OUT_{cond}}}$) and the evaporator outlet superheating (T_{SH}) using compressor speed (ω) and valve opening degree (z) as control actions. The framework was tested on an emulator based on the high-fidelity system model used in the controller. The controller was evaluated across multiple setpoints and objective function weightings (R and Q, Eq. (14)), demonstrating consistent performance. A representative scenario is presented to illustrate the results. Tables 1 and 2 show the initial conditions set for the states of the MBM model of the evaporator (Eq. (1)) and the condenser (Eq. (2)).

Table 1. Initial values of the states X_{evap} for the MBM evaporator model

Component	$L_{TP_{evap}}$ (m)	p_{evap} (kPa)	$h_{OUT_{evap}}$ (kJ kg^{-1})	$T_{W_{TP_{evap}}}$(°C)	$T_{W_{SHV_{evap}}}$ (°C)
Evaporator	46.17	65.66	2660.28	89.45	95.05

Table 2. Initial values of the states X_{cond} for the MBM condenser model

Component	$L_{SCL_{cond}}$ (m)	$L_{TP_{cond}}$ (m)	p_{cond} (kPa)	$h_{OUT_{cond}}$ (kJ kg^{-1})	$T_{W_{SCL_{cond}}}$ (°C)	$T_{W_{TP_{cond}}}$(°C)	$T_{W_{SHV_{cond}}}$ (°C)
Condenser	0.83	48.91	1597.82	823.23	267.61	198.44	195.46

In relation to the system inputs, the initial values are reported in Table 3 (Eq. (7)).

Table 3. Initial values of the input U for the MBM models

$\dot{m}_{SEC_{evap}}$ (kg/s)	$T_{SEC_{IN_{evap}}}$(°C)	$\dot{m}_{SEC_{cond}}$(kg/s)	$T_{SEC_{IN_{cond}}}$(°C)	z (-)	ω (rps)
1.61	115	1.33	162.5	0.51	129.80

Under these initial conditions, setpoint targets were imposed for the secondary fluid outlet temperature from the condenser ($T_{\mathrm{SEC\_OUT\_cond}}$) at 196 °C and for the superheating at the evaporator outlet (T_{SH}) at 1.5 °C. The weighting matrix Q and the control effort weighting R (Eq. (14)) were calibrated to achieve fast control response without inducing excessive oscillations in the outputs. The optimal values for Q were 3 and 28 for the two outputs, in the order of T_{SH} and $T_{\mathrm{SEC\_OUT\_cond}}$, respectively, while for R the corresponding values were 5 and 4 for the same outputs. The controller was then tested with a PH of 5 minutes and a control timestep of 1 minute ($\Delta \mathrm{k}_{\mathrm{MPC}}$). Figure 4 shows the control results. The controller is seen to effectively reach the setpoints of both outputs relatively quickly (within 15 minutes), without inducing excessive oscillations in either the outputs or the control variables.

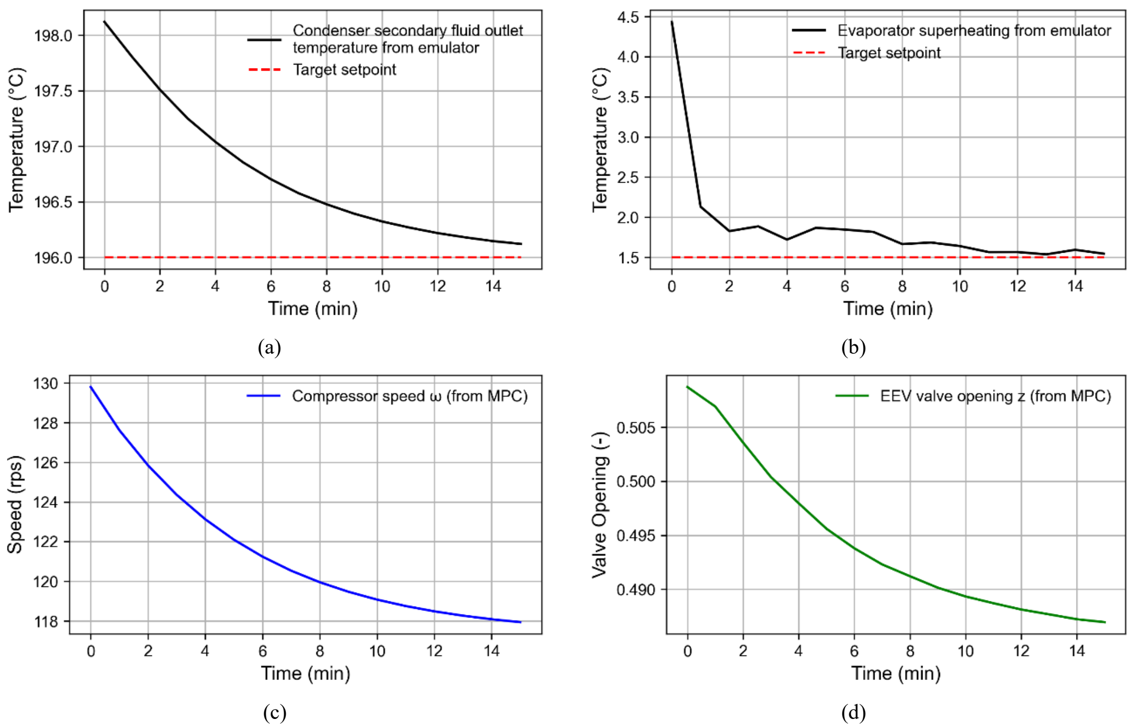

Figure 4. MPC control results: (a) Comparison between the condenser secondary fluid outlet temperature and its setpoint, (b) Comparison between the evaporator superheating and its setpoint, (c) Compressor speed (ω) implemented by the MPC, and (d) EEV valve opening (z) implemented by the MPC.

As shown in Figure 4, the control is highly effective. However, to achieve these results in a control setup that is feasible for real-world applications, it was necessary to implement black-box models based on polynomial regressions (subsection 2.2), to decouple from *CoolProp*. Preliminary tests using *CoolProp* to maintain the fluid properties revealed that the solution time for a prediction horizon of 5 minutes was always above 100 seconds. This is incompatible with an on-board control system for HP. With the introduction of polynomial correlations, the computation time was significantly reduced. The average solution time of the first simulation phase of the high-fidelity model (Figure 2) is now 16.8 seconds, corresponding to a speed-up of approximately 83.2% compared to the 100 seconds required using *CoolProp*. It should be emphasized, however, that in order to obtain reliable results, the polynomial regressions must have a very low error. In the present case, the percentage error was consistently kept below 0.5%.

From a quantitative perspective, the MPC framework drives both the superheating temperature and the condenser outlet temperature toward their respective setpoints, with the relative weighting factors R and Q (Eq. (14)) allowing prioritized convergence. In terms of performance, the superheating temperature reaches within

0.5 °C of its setpoint after approximately 2 minutes, while the condenser outlet temperature achieves a difference from its setpoint of less than 0.5 °C after about 8 minutes.

4.2 Limitations and Future Work

This study focuses on the development of a computationally efficient low-level MPC framework suitable for integration with high-level supervisory control. It presents an initial configuration of the controller, demonstrating feasibility and implementation methodology. While preliminary and subject to certain limitations, the results highlight the potential of the approach and indicate directions for future work, which are discussed in this section.

Considering the limitations of this study, it should be noted that validation was performed using an emulator derived from the same high-fidelity model employed for controller development. This approach may slightly overestimate real-world performance due to the absence of model–plant mismatch. In addition, simulations were conducted using pure water as the refrigerant rather than the actual ammonia–water mixture. This simplification was necessary to reduce computation time and allow a clear demonstration of the feasibility of the framework.

Future work will focus on extending validation using alternative high-fidelity models, such as finite-volume simulations implemented in Modelica, to assess controller robustness. Experimental testing and dynamic setpoint scenarios, in which reference trajectories vary over time, will also be explored. Furthermore, the low-level MPC will be evaluated within hierarchical control architectures, integrated with a high-level supervisory controller (e.g., predictive or optimal), particularly in residential HVAC applications, to assess performance in a fully coordinated system. Finally, future studies will also consider the actual ammonia–water mixture to provide a more realistic assessment of controller performance.

Overall, however, despite these limitations, the study demonstrates the relevance and potential of the proposed approach, showing that a computationally efficient low-level MPC can be developed and integrated into high-level control architectures, paving the way for practical and flexible heat pump management.

5. Conclusions

This study introduced a novel Model Predictive Control architecture designed to replace conventional on-board controllers in heat pump systems. The proposed framework demonstrates how a state-space formulation of the heat pump can be effectively adapted for control purposes. A black-box modeling approach was employed to capture the thermodynamic behavior of the refrigerant, while linearization techniques were used to enhance computational efficiency without compromising model accuracy. Building upon these elements, an Model Predictive Control scheme was developed based on a linearized vapor-compression cycle model with Moving-Boundary heat exchanger representations and implemented for a high-temperature heat pump. The control strategy was tested in a simulation environment, showing accurate setpoint tracking and stable operation under the conditions considered.

The results obtained confirm the effectiveness and feasibility of the proposed control framework, providing a solid foundation for further development. Future work will focus on experimental validation and on testing the controller with different high-fidelity emulators or real systems, as well as on extending its application to dynamic setpoint tracking and hierarchical control architecture. Overall, this research provides a first step toward the integration of advanced predictive control in commercial heat pumps, highlighting its potential to enhance performance and flexibility compared to conventional control solutions.

Acknowledgements

This work was supported by HBC.2022.0539 – UPHEAT-INES-2: Upgraded High Temperature Heat in Energy Intensive Sectors 2.0 [29]. The authors would like to thank Shahzaib Abbasi for his valuable support.

References

[1] European Commission. Communication from the Commission: The European Green Deal. Brussels: European Commission; 2021. Available at: ec.europa.eu/info/strategy/priorities-2019-2024/european-green-deal_en

[2] Fischer D, Madani H. On heat pumps in smart grids: A review. *Renewable and Sustainable Energy Reviews* 2017;70:342–357. doi.org/10.1016/j.rser.2016.11.182

[3] Jensen SØ, Marszal-Pomianowska A, Lollini R, Pasut W, Knotzer A, Engelmann P, Stafford A, Reynders G. IEA EBC Annex 67 Energy Flexible Buildings. *Energy and Buildings* 2017;155:25–34. doi.org/10.1016/j.enbuild.2017.08.044

[4] Luo Z, Peng J, Cao J, Yin R, Zou B, Tan Y, Yan J. Demand flexibility of residential buildings: Definitions, flexible loads, and quantification methods. *Engineering* 2022;16:123–140. doi.org/10.1016/j.eng.2022.01.010

[5] Li H, Wang Z, Hong T, Piette MA. Energy flexibility of residential buildings: A systematic review of characterization and quantification methods and applications. *Advances in Applied Energy* 2021;3:100054. doi.org/10.1016/j.adapen.2021.100054

[6] He Y, Zhou H, Fahimi F. Modeling and demand-based control of responsive building envelope with integrated thermal mass and active thermal insulations. *Energy and Buildings* 2022;276:112495. https://doi.org/10.1016/j.enbuild.2022.112495

[7] Tunçbilek E, Yıldız Ç, Arıcı M, Ma Z, Awan MB. Thermal energy storage for enhanced building energy flexibility. In: Ma Z, Arıcı M, Shahsavar A, editors. *Building Energy Flexibility and Demand Management*. Academic Press; 2023. p. 89–119. doi.org/10.1016/B978-0-323-99588-7.00004-3

[8] Liu Z, Zhang X, Sun Y, Zhou Y. Advanced controls on energy reliability, flexibility and occupant-centric control for smart and energy-efficient buildings. *Energy and Buildings* 2023;297:113436. doi.org/10.1016/j.enbuild.2023.113436

[9] Drgoňa J, Arroyo J, Cupeiro Figueroa I, Blum D, Arendt K, Kim D, Perarnau Ollé E, Oravec J, Wetter M, Vrabie DL, Helsen L. All you need to know about model predictive control for buildings. *Annual Reviews in Control* 2020;50:190–232. doi.org/10.1016/j.arcontrol.2020.09.001

[10] Afram A, Janabi-Sharifi F. Theory and applications of HVAC control systems – A review of model predictive control (MPC). *Building and Environment* 2014;72:343–355. doi.org/10.1016/j.buildenv.2013.11.016

[11] Zhao Z, Wang C, Wang B. Adaptive model predictive control of a heat pump-assisted solar water heating system. *Energy and Buildings* 2023;300:113682. doi.org/10.1016/j.enbuild.2023.113682

[12] Strauch P, Wang W, Langner F. Model predictive control for demand flexibility of a residential building with multiple distributed energy resources. *Energy and Buildings* 2024;305:113884. doi.org/10.1016/j.enbuild.2023.113884

[13] Zong Y, Su W, Wang J, Rodek JK, Jiang C, Christensen MH, You S, Zhou Y, Mu S. Model Predictive Control for Smart Buildings to Provide the Demand Side Flexibility in the Multi-Carrier Energy Context: Current Status, Pros and Cons, Feasibility and Barriers. *Energy Procedia* 2019;158:3026–3031. doi.org/10.1016/j.egypro.2019.01.981

[14] Zong Y, Su W, Wang J, Rodek JK, Jiang C, Christensen MH, You S, Zhou Y, Mu S. Model Predictive Control for Smart Buildings to Provide the Demand Side Flexibility in the Multi-Carrier Energy Context: Current Status, Pros and Cons, Feasibility and Barriers. *Energy Procedia* 2019;158:3026–3031. doi.org/10.1016/j.egypro.2019.01.981

[15] Péan T, Costa-Castelló R, Fuentes E, Salom J. Experimental Testing of Variable Speed Heat Pump Control Strategies for Enhancing Energy Flexibility in Buildings. *IEEE Access* 2019;7:37071–37087. doi.org/10.1109/ACCESS.2019.2903084

[16] Evens M, Arteconi A. Influence of internal control simplifications in heat pump system modelling for energy flexibility evaluations. In: *Proceedings of Building Simulation 2021: 17th Conference of IBPSA*; 2021. p. 1212–1219. doi.org/10.26868/25222708.2021.30214

[17] He XD, Liu S, Asada HH. Modeling of vapor compression cycles for multivariable feedback control of HVAC systems. *Journal of Dynamic Systems, Measurement, and Control* 1997;119(2):183–91. doi.org/10.1115/1.2801231

[18] He XD, Liu S, Asada HH, Itoh H. Multivariable control of vapor compression systems. *HVAC&R Research* 1998;4(3):205–30. doi.org/10.1080/10789669.1998.10391401

[19] Liu S, He XD, Asada H, Itoh H, Nakagawa K. Multivariable control of vapor compression cycles: coordination of compressor and expansion valve. *IFAC Proceedings Volumes* 1996;29(1):5989–94. doi.org/10.1016/S1474-6670(17)58640-1

[20] Rasmussen BP. Dynamic modeling for vapor compression systems—Part I: Literature review. *HVAC&R Research* 2012;18(5):934–55. doi.org/10.1080/10789669.2011.582916

[21] Rasmussen BP, Shenoy B. Dynamic modeling for vapor compression systems—Part II: Simulation tutorial. *HVAC&R Research* 2012;18(5):956–73. doi.org/10.1080/10789669.2011.582917

[22] Rasmussen BP, Alleyne AG. Dynamic modeling and advanced control of air conditioning and refrigeration systems. 2006.
[23] Bendapudi S, Braun JE, Groll EA. A comparison of moving-boundary and finite-volume formulations for transients in centrifugal chillers. *International Journal of Refrigeration* 2008;31(8):1437–52. doi.org/10.1016/j.ijrefrig.2008.03.006
[24] Bell IH, Wronski J, Quoilin S, Lemort V. Pure and pseudo-pure fluid thermophysical property evaluation and the open-source thermophysical property library CoolProp. *Industrial & Engineering Chemistry Research* 2014;53(6):2498–508. doi.org/10.1021/ie4033999
[25] Mugnini A, Evens M, Arteconi A. Model predictive controls for residential buildings with heat pumps: Experimentally validated archetypes to simplify the large-scale application. *Energy and Buildings* 2024;320:114632. doi.org/10.1016/j.enbuild.2024.114632
[26] G. L. Wedekind, B. L. Bhatt, and B. T. Beck, “A system mean void fraction model for predicting various transient phenomena associated with two-phase evaporating and condensing flows,” *International Journal of Multiphase Flow*, vol. 4, no. 1, pp. 97–114, Mar. 1978. doi:10.1016/0301-9322(78)90029-0.
[27] W. Li, “Simplified modeling analysis of mass flow characteristics in electronic expansion valve,” Applied Thermal Engineering, vol. 53, no. 1, pp. 8–12, 2013. doi:10.1016/j.applthermaleng.2012.12.03.
[28] J. Liu, W. J. Wei, G. L. Ding, C. Zhang, M. Fukaya, K. Wang, and T. Inagaki, “A general steady-state mathematical model for fin-and-tube heat exchanger based on graph theory,” International Journal of Refrigeration, vol. 27, no. 9, pp. 965–973, 2004. doi: 10.1016/j.ijrefrig.2004.06.008.
[29] Moonshot Flanders. (2025). *UpHeat-INES-2: Upgraded high temperature heat in energy intensive sectors 2.0* (Progetto HBC.2022.0539). www.moonshotflanders.be/en/projects/upheat-ines-2
[30] Vahterus, *Custom-made Plate & Shell Heat Exchanger Solution*, available online: vahterus.com/, accessed November 11, 2025.
[31] SWEP, *Challenge Efficiency*, available online: www.swep.net/, accessed November 11, 2025.
[32] Verein Deutscher Ingenieure (VDI)-Gesellschaft Verfahrenstechnik und Chemieingenieurwesen (GVC) (Eds.). *VDI-Wärmeatlas*. 11. ed., Springer-Verlag Berlin / Heidelberg, 2013. DOI: 10.1007/978-3-642-19981-3.
[33] Shah M. Improved correlation for heat transfer during condensation in conventional and mini/micro channels. *International Journal of Refrigeration* 2019;98:222–237. doi:10.1016/j.ijrefrig.2018.07.037
[34] Shah M. New general correlation for heat transfer during saturated boiling in mini and macro channels. *International Journal of Refrigeration* 2022;137:103–116. doi:10.1016/j.ijrefrig.2022.02.019